Electrostatic-magnetic-hybrid thrust generation in central‐cathode electrostatic thruster (CC‐EST)

Akihiro Sasoh*, Hayato Kasuga, Yoshiya Nakagawa, Toshihiro Matsuba, Daisuke Ichihara, and Akira Iwakawa

Department of Aerospace Engineering, Nagoya University, Nagoya 464‐8603, Japan

ARTICLE INFO

Keywords: Electric propulsion, Electrostatic acceleration, Electromagnetic acceleration, Thrust

ABSTRACT

The thrust characteristics of electrostatic-magnetic hybrid acceleration have been obtained in the central–cathode electrostatic thruster (CC-EST), which has a diverging magnetic nozzle and injects propellant through an annular slit on the inner surface of a ring anode. The electrostatic and electromagnetic contributions are evaluated by fitting experimentally measured thrust characteristics to formulae derived for steady-state, quasi-neutral plasma flows. The thrust is composed of two terms: one corresponds to the electrostatic acceleration interfaced by the magnetized electrons, the other to electromagnetic acceleration yielding a kinetic energy of swirl motion that is converted to that of axial motion in the diverging magnetic nozzle. The thrust performances of three thrusters having an axisymmetric shape with a hollow cathode on the centre axis and a diverging, applied magnetic field are examined. While only an electromagnetic thrust component is obtained in the conventional applied-field magneto-plasma-dynamics thruster, the other two, CC‐ESTs, exhibit comparable, electrostatic, and electromagnetic thrust components, and thus improve thrust performance.

Nomenclature

Abbreviations

CV control volume

*Corresponding author: akihiro.sasoh@mae.nagoya‐u.ac.jp (A. Sasoh)

Variables

$\mathbf{B}$	magnetic field
$\mathbf{B}_\mathrm{a}$	applied magnetic field
$\bar{B}_\mathrm{a}$	representative value of applied magnetic field at coil/magnet centre on the axis
$\bar{B}_{\mathrm{a,c}}$	critical value of $\bar{B}_\mathrm{a}$
$\tilde{\mathrm{D}} / \mathrm{D}t$	defined by Eq. (5)
e	elementary charge
$\mathbf{E}$	electric field
$\mathbf{j}$	current density
$\mathbf{j}_\mathrm{d}$	discharge current
$\mathbf{j}_\mathrm{i}$	induced current
F	thrust
L	length of acceleration region
L_a	length of ring anode exposed in acceleration region
m	atomic mass
$\dot{m}$	mass flow rate
n	number density
p	pressure
R_a	anode inner radius
(r,θ,z)	cylindrical coordinates
U	exhaust speed of propellant
$\mathbf{u}$	flow velocity
$\mathbf{u}_{r,z}$	translational flow velocity
$\mathbf{u}_\theta$	azimuthal flow velocity
V_d	discharge voltage
α, α', $\alpha_{\mathrm{ES}}, \alpha_{\mathrm{EM}}, \beta_1$, β_2	coefficients
ρ	density

$\omega_e \tau_e$ electron Hall parameter

$\overline{( )}$ representative value

Subscripts

a anode or applied

c cathode or critical

EM electromagnetic

ES electrostatic

1. Introduction

Electric space propulsion is defined as a method of space propulsion using electrical power. Its usefulness in space is rapidly being enhanced with growing space activities from large-payload, all-electric missions [1,2] to small ones even for CubeSats. [3-5] Its plasma acceleration principle is usually subdivided into three types, electrostatic, electromagnetic, and electrothermal accelerations. [6,7] In electrostatic–acceleration–type thrusters, the ions can gain an energy corresponding to an applied voltage. In ion thrusters, the electrons are not introduced to the ion acceleration region, which is sandwiched by grids having different electrical potentials; only the ions experience a propulsive force, which is a thrust. This configuration is favourable to obtain high thrust efficiency because with appropriate beam optics, the momentum transfer becomes collision–free. However, thrust density is limited due to Child–Langmuir's space–charge limit. [8] In Hall thrusters [9-12] and other similar types of thrusters including cylindrical Hall thrusters [13,14], high-efficiency multistage plasma (HEMP) thrusters [15,16] and diverging-magnetic-field electrostatic thrusters (DM‑EST) [17-19], the ions are accelerated in quasi-neutral plasma. Without the space–charge limit, they can potentially achieve an even higher thrust density than that of ion thrusters along with reasonable thrust efficiency. In electromagnetic–acceleration-type thrusters, which are often represented by magneto-plasma-dynamics (MPD) thrusters, the quasi‑neutral plasma experiences a Lorentz force produced by the interactions between a discharge current and an applied‑ and/or self-induced magnetic field. Because most of the discharge current is a result of the motion of electrons, the momentum transfer mechanisms from the electrons to the ions must exist. On the one hand, if such momentum transfer is caused by particle collisions, the ions can obtain a

kinetic energy even higher than that corresponding to a discharge voltage; its thrust density can be higher than that of a Hall thruster. [20-22] On the other hand, such collisional momentum transfer is accompanied by poor energy transfer efficiency, as well as poor thrust efficiency. In electrothermal–acceleration-type thrusters, which are often represented by arcjet, the propellant gains propulsive kinetic energy from Joule heating. In this case, high thrust density can be achieved, yet with modest thrust efficiency.

The ideal thrust produced by ion thrusters for singly charged propellant is formulated readily from the energy conservation equation—the ions gain a kinetic energy from the applied electrostatic potential drop [7,23]. This electrostatic thrust is in proportion with the effective ion beam current and then the propellant flow rate. The thrust production mechanisms in Hall thrusters are rather complicated compared to ion thrusters because an electrostatic force is exerted on the electrons in $\mathbf{E}\times\mathbf{B}$ drift motion, then being transferred to the ions through a macroscopic electric field; the ideal thrust; however, has the same form as that of ion thrusters, in which the thrust is in proportion to the ion flow rate and the square root of the discharge voltage. The total efficiency based on practical performance is factored by coefficients due to beam divergence and various efficiencies [7].

In electromagnetic–acceleration-type thrusters, if the distributions of discharge current density, $\mathbf{j}$, and of magnetic field, $\mathbf{B}$, are known, the Lorentz force produced by their interaction can be obtained by the volume integration of the body force, $\mathbf{j}\times\mathbf{B}$. Here, assume an axisymmetric thruster configuration. The formula for self–magnetic thrust, that is produced by the interaction between the discharge current and the magnetic field induced by the discharge current itself, is obtained in a closed form, [6,24] and has been experimentally validated. [6,25] However, when an external magnetic field is applied in the axial and radial directions, the Lorentz force has an azimuthal component, exerting a torque onto the propellant flow thereby inducing its swirl motion. In order to generate a thrust, the kinetic energy of the swirl motion needs to be converted to that of the axial motion. Such a thrust component cannot be obtained in a closed form if appropriate assumptions are not imposed. Fradkin et al. [26] obtained a thrust formula for the swirl acceleration by the rigid rotator model in which the local angular velocity of the propellant depends only on the axial coordinate. As will be demonstrated later, this formula describes experimentally measured thrust characteristics only in a qualitative manner.

In electrothermal–acceleration-type thrusters, the thrust depends on the energy conversion rate from the electrical power input to the kinetic energy of the plasma flow, that is the thrust efficiency or thermal efficiency. Since the efficiency depends on various thruster operation parameters including the discharge current, discharge voltage, propellant mass flow rate, and thruster geometry, it is difficult to give a thrust formula in a closed form. Hügel [27] proposed that the thrust of an arcjet thruster, a typical electrothermal–acceleration-type thruster, is composed of the electrothermal and self-electromagnetic thrust components; in the former the electrothermal thrust is assumed to scale with the square root of the product of the discharge current and the propellant mass flow rate. Tikhonov et al. [28,29] proposed an empirical thrust formula containing a self-magnetic, applied-magnetic, and electro-thermal thrust component. Sasoh and Arakawa [30] proposed a thrust formula for applied-field MPD thruster based on the energy conservation equation. Sasoh [31] added an electrothermal component to Sasoh & Arakawa's formula. Coletti [32] proposed a thrust formula in applied-field MPD thruster by assuming the plasma motion through a diverging magnetic nozzle.

In the above-mentioned categorization, the electrostatic and electromagnetic accelerations are regarded as different types although they share common features. Sasoh et al. [33] experimentally demonstrated that the central-cathode electrostatic thruster (CC–EST) in which a slowly diverging magnetic field is applied between a ring anode and an on-axis hollow cathode exhibited both electrostatic and electromagnetic thrust characteristics. However, their mutual relationship has not been quantified. In the hybrid acceleration, it is expected that the thrust density becomes higher than that only by electrostatic acceleration, and the thrust efficiency becomes higher than that only by electromagnetic acceleration. However, such an electrostatic-magnetic hybrid thrust generation has not been well recognized as a promising method in electric space propulsion. In order to further investigate this technology, it is important that the respective thrust components, electrostatic and electromagnetic, be quantified. The purpose of this study is to quantify the electrostatic–magnetic hybrid thrust components in the CC–EST operations by fitting formulae derived based on magnetoplasmadynamics to experimentally measured thrust characteristics to demonstrate the usefulness of this technology.

2. Thruster configuration

Figure 1 schematically illustrates the configurations of plasma acceleration investigated in this study. Assume steady-state, axisymmetric, quasi-neutral plasma flows in which electric and magnetic fields are applied. Figure 1a corresponds to the electrostatic (Hall) acceleration. Using cylindrical coordinates, (r,θ,z), an electric field, $\mathbf{E}$, is formed between the anode and cathode in the (r,z) directions, which will hereafter be referred to as the translational direction. The electric field is assumed to be formed normal to the applied magnetic field, $\mathbf{B}_\mathrm{a}$, which also has (r,z) components. An azimuthal current, $\mathbf{j}_\mathrm{i}$, is induced by the $\mathbf{E}\times\mathbf{B}$ drift motion of the electrons. Hence, the body force, $\mathbf{f}$, yields

$$\mathbf{f}=\mathbf{j}_\mathrm{i}\times\mathbf{B}_\mathrm{a}=-ne\frac{\left(\mathbf{E}\times\mathbf{B}_\mathrm{a}\right)}{\left|\mathbf{B}_\mathrm{a}\right|^2}\times\mathbf{B}_\mathrm{a}=ne\mathbf{E} \tag{1}$$

This is the basic principle of electrostatic ion acceleration in Hall thrusters, which is well documented. [7] Neglecting pressure gradients, the ions are accelerated by the electric fields through the magnetized electrons. If the applied electric potential is utilized fully to accelerate the ions, they can obtain a kinetic energy equivalent to a discharge voltage. That is, the kinetic energy of the accelerated ions cannot exceed that value. This principle is also applicable to cylindrical Hall thrusters and similar types. [13-16,19,34-36]

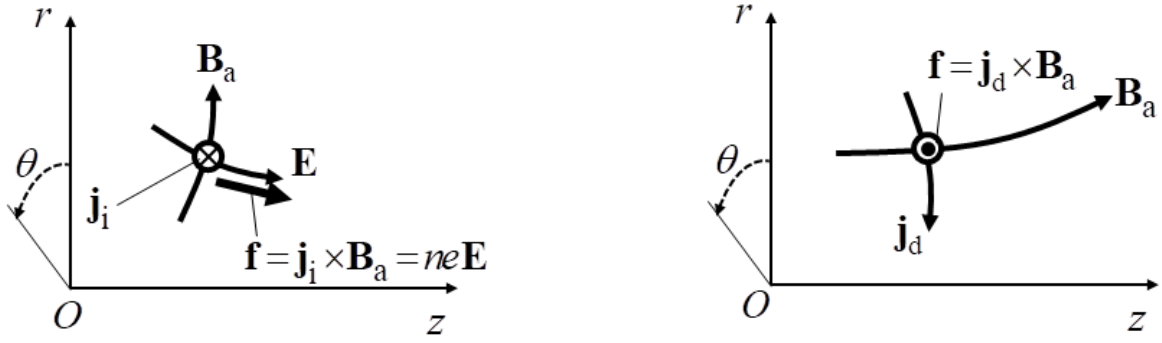

a) Electrostatic (Hall) acceleration b) Electromagnetic (swirl) acceleration

Fig. 1 Configurations of quasi-neutral plasma acceleration in the cylindrical coordinates (r,θ,z).

Figure 1b schematically illustrates the electromagnetic acceleration executed in applied-field MPD thrusters [37-46]. Neglecting the contribution of a self-induced magnetic field, a Lorentz force, $\mathbf{f}$, is exerted in the azimuthal (θ) direction through the interaction between a discharge current, $\mathbf{j}_\mathrm{d}$, and $\mathbf{B}_\mathrm{a}$, both of which have only (r,z) components. The plasma flow gains kinetic energy in its swirl motion through the work done by the torque due to this body force. An important difference from the above-mentioned electrostatic acceleration is that in this swirl acceleration, the kinetic energy of the ions is not limited by the value equivalent to the discharge voltage. Depending on the magnitudes of $\mathbf{j}_\mathrm{d}$ and $\mathbf{B}_\mathrm{a}$, and a propellant mass flow rate, $\dot{m}$, an even higher kinetic energy is achievable. Although the mechanisms of the swirl acceleration are physically clear, the corresponding thrust has been formulated to a limited extent because it depends on the spatial distributions of plasma flow parameters. Fradkin et al. [26] formulated the thrust due to the swirl acceleration by assuming that the plasma in a hollow cylinder with inner and outer radii of R_c and R_a. respectively, acted as a rigid rotator, in which the angular velocity is kept uniform at an axial location, z, and the kinetic energy of the rotation is fully converted to the axial kinetic energy after the expansion through a diverging magnetic nozzle. Under these assumptions, the thrust is given in a closed form as

$$F = \frac{1}{\sqrt{2}} J_\mathrm{d} B_\mathrm{a} R_\mathrm{a} \frac{1-\left(\frac{R_\mathrm{c}}{R_\mathrm{a}}\right)^2}{\sqrt{1+\left(\frac{R_\mathrm{c}}{R_\mathrm{a}}\right)^2}} \simeq \frac{1}{\sqrt{2}} J_\mathrm{d} B_\mathrm{a} R_\mathrm{a} \left\{1-\frac{3}{2}\left(\frac{R_\mathrm{c}}{R_\mathrm{a}}\right)^2\right\} \qquad (2)$$

This formula adequately represents the experimentally measured thrust performance of the applied-field MPD thrusters in a qualitative manner [47], but not in a quantitative manner; typically, the experimental coefficient to $J_\mathrm{d} B_\mathrm{a} R_\mathrm{a}$ is approximately 30% of that given by Eq. (2). [42,48] Sasoh & Arakawa [30,41] and Sasoh [31] proposed the thrust formulae of the applied-field MPD thrusters in which the swirl, Hall, self-magnetic, and even electrothermal accelerations are taken into account. In their formula, the thrust component of the Hall acceleration, which was produced by the interaction between the azimuthally-induced current

and the applied, magnetic field, was scaled with a product of $(\omega_e\tau_e)J_dB_a$. Since the electron Hall parameter, $(\omega_e\tau_e)$, was proportional to B_a, this thrust component was proportional to $J_dB_a^2$. Their formula, derived based on an energy conservation equation under the above assumption, had a complicated form and had not been experimentally validated under wide operating conditions. Coletti [32] proposed a thrust formula for the applied‑field MPD thruster by considering plasma expansion through a magnetic nozzle. Tikhonov et al. [28,29] suggested an empirical formula comprising the gas dynamic, Hall, and self-magnetic thrust components. Owing to its simplicity, it has been most referred to in previous studies although the values of coefficients used were not supported theoretically. Albertoni et al. also suggested a phenomenological thrust formula combining self-field and applied-field (swirl) thrusts. [49] Myers [42] experimentally investigated the scaling effects on the specific impulse, discharge voltage, and thrust efficiency in the applied-field MPD thrusters. He concluded that the anode power deposition had the largest efficiency loss, which could be decreased with increasing the applied–field strength and anode radius.

Sasoh et al. [33] reported the electrostatic-magnetic hybrid thrust performance of the central-cathode electrostatic thruster (CC-EST), comprising a ring anode, a hollow cathode on the centre axis, and an applied diverging magnetic field. They demonstrated that with the near-anode ionization scheme, in which the propellant was injected from a circular slit along the anode's inner surface, a favourable thrust performance was obtained. Boxberger and Herdrich [50] and Wang et al. [51] reported favourable results using similar thruster configurations, yet as applied-field MPD thrusters. In this study, the thrust characteristics of the CC‑EST will be modelled and formulated such that the experimentally obtained, hybrid thrust characteristics have quantitative significance.

Figure 2 schematically illustrates the basic thruster configuration of the CC‑EST investigated in this study. It comprises an anode having a ring shape, cathode, magnet, and insulator. All the parts have an axisymmetric shape on the cylindrical coordinates (r,θ,z) and are coaxially set. A diverging magnetic field is applied using the magnet. A discharge voltage, V_d, is applied between the anode and cathode. The propellant, an inert gas, is supplied through the annular slit

along the anode's inner surface, with a mass flow rate of $\dot{m}_a$. The cathode operation gas is supplied with a mass flow rate of $\dot{m}_c$ through the cathode keeper orifice to the plasma acceleration region. Here, we neglect the contribution of the cathode working gas to the thrust generation. The insulator fills the inter-electrode space, except for the slit for the propellant injection. The propellant injected from the slit is expected to be ionized near the anode and accelerated in the acceleration region where the electric ($\mathbf{E}$) and magnetic ($\mathbf{B}_a$) fields are applied.

In an end-Hall ion source, [52] the working gas is injected behind the anode such that the ion beam is uniformly distributed downstream. Conversely, in the CC-EST, the near-anode ionization scheme encourages efficient ion acceleration by utilizing the applied electric voltage between the electrodes. In cylindrical Hall thrusters, [13,34-36] a similar diverging magnetic field is applied. However, the arrangement of an anode and the magnetic field is somehow similar to that of a conventional SPT-type Hall thruster [7,9,10,53] and the high-efficiency multi-stage plasma (HEMP) thruster; [15,16,54] the anode is located on the upstream side of the acceleration region, with its surface facing the thrust direction. The applied magnetic field on the anode surface has a large radial component.

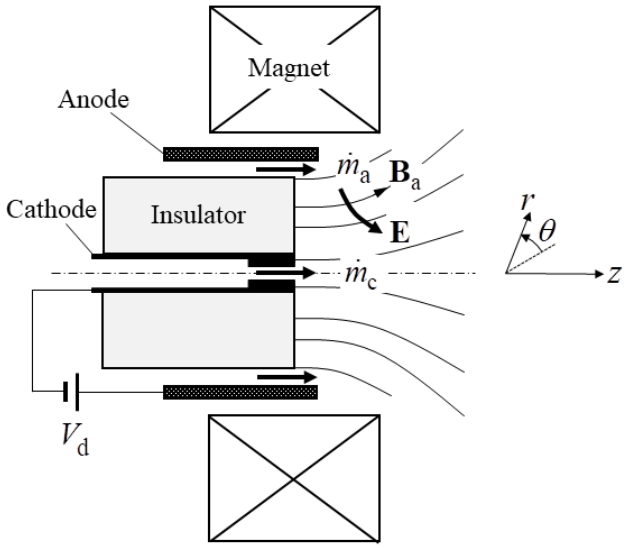

Fig. 2 Basic thruster configuration of CC-EST.

3. Plasma acceleration model and thrust formulae

3.1 Fundamental equations

Here, assume the steady-state, inviscid, quasi-neutral plasma flow governed by the Euler equation with body-force source terms. [55]

$$\rho(\mathbf{u}\cdot\nabla)\mathbf{u} = -\nabla p + \mathbf{j}\times\mathbf{B} \tag{3}$$

As is found in fundamental textbooks dealing with fluid dynamics such as [56], on (r,θ,z) cylindrical coordinates, see Fig. 2, the convective acceleration terms are given as

$$\mathbf{u}\cdot\nabla\mathbf{u} = \begin{pmatrix} u_r\dfrac{\partial u_r}{\partial r} + \dfrac{u_\theta}{r}\dfrac{\partial u_r}{\partial \theta} - \dfrac{u_\theta^2}{r} + u_z\dfrac{\partial u_r}{\partial z} \\ u_r\dfrac{\partial u_\theta}{\partial r} + \dfrac{u_\theta}{r}\dfrac{\partial u_\theta}{\partial \theta} + \dfrac{u_r u_\theta}{r} + u_z\dfrac{\partial u_\theta}{\partial z} \\ u_r\dfrac{\partial u_z}{\partial r} + \dfrac{u_\theta}{r}\dfrac{\partial u_z}{\partial \theta} + u_z\dfrac{\partial u_z}{\partial z} \end{pmatrix} \tag{4}$$

Defining

$$\frac{\tilde{\mathrm{D}}}{\mathrm{D}t} \equiv u_r\frac{\partial}{\partial r} + \frac{u_\theta}{r}\frac{\partial}{\partial \theta} + u_z\frac{\partial}{\partial z}, \tag{5}$$

Equation (4) yields

$$\mathbf{u}\cdot\nabla\mathbf{u} = \begin{pmatrix} \dfrac{\tilde{\mathrm{D}}u_r}{\mathrm{D}t} - \dfrac{u_\theta^2}{r} \\ \dfrac{\tilde{\mathrm{D}}u_\theta}{\mathrm{D}t} + \dfrac{u_r u_\theta}{r} \\ \dfrac{\tilde{\mathrm{D}}u_z}{\mathrm{D}t} \end{pmatrix}. \tag{6}$$

Neglecting the self-induced magnetic field, B_θ, the magnetic field has only the applied components.

$$\mathbf{B}_\mathrm{a} \equiv \begin{pmatrix} B_r \\ 0 \\ B_z \end{pmatrix} \tag{7}$$

The current density, $\mathbf{j}$, is the sum of the discharge ($\mathbf{j}_\mathrm{d}$) and induced ($\mathbf{j}_\mathrm{i}$) terms.

$$\mathbf{j} = \mathbf{j}_\mathrm{d} + \mathbf{j}_\mathrm{i}, \tag{8}$$

$$\mathbf{j}_{\mathrm{d}} \equiv \begin{pmatrix} j_r \\ 0 \\ j_z \end{pmatrix}, \tag{9}$$

$$\mathbf{j}_{\mathrm{i}} = \begin{pmatrix} 0 \\ j_\theta \\ 0 \end{pmatrix}, \tag{10}$$

where $\mathbf{j}_{\mathrm{i}}$ has the azimuthal current component that is induced by the $\mathbf{E}\times\mathbf{B}$ drift motion of the electrons. Usually, in high specific impulse systems, the contribution of electrothermal acceleration in which a static enthalpy is converted to the kinetic energy of the plasma flow through negative pressure gradient is neglected. For example, in CC-EST-2 thruster that will be shown later, according to Langmuir probe (double probe) measurement, the electron temperature level in the acceleration system is of the order of 10 eV, which is about 5 % of the typical discharge voltage of 200 V that should ideally be equivalent to the ion kinetic energy. Therefore, in the present analyses, we neglect the effect of the electrothermal acceleration and the pressure, p in Eq. (3). Using Eq. (6), the components in Eq. (3) are expressed as follows:

$$\rho\left(\frac{\tilde{\mathrm{D}}u_r}{\mathrm{D}t} - \frac{u_\theta^2}{r}\right) = \mathbf{j}_{\mathrm{i}} \times \mathbf{B}_{\mathrm{a}}\big|_r = j_\theta B_z, \tag{11}$$

$$\rho\left(\frac{\tilde{\mathrm{D}}u_\theta}{\mathrm{D}t} + \frac{u_r u_\theta}{r}\right) = \mathbf{j}_{\mathrm{d}} \times \mathbf{B}_{\mathrm{a}}\big|_\theta, \tag{12}$$

$$\rho\frac{\tilde{\mathrm{D}}u_z}{\mathrm{D}t} = \mathbf{j}_{\mathrm{i}} \times \mathbf{B}_{\mathrm{a}}\big|_z = -j_\theta B_r . \tag{13}$$

Here, we assume that the induced current is in proportion to the discharge current.

$$\left|\mathbf{j}_{\mathrm{i}}\right| \equiv \alpha_{\mathrm{ES}}\left|\mathbf{j}_{\mathrm{d}}\right|. \tag{14}$$

From Eqs. (11) and (13),

$$\frac{1}{2}\rho\frac{\mathrm{D}u_{r,z}^2}{\mathrm{D}t} = \left(\mathbf{j}_{\mathrm{i}} \times \mathbf{B}_{\mathrm{a}}\right)\cdot\mathbf{u}_{r,z} + \rho\frac{u_r u_\theta^2}{r}, \tag{15}$$

where a translational velocity, $\mathbf{u}_{r,z}$, is defined as

$$\mathbf{u}_{r,z} \equiv \begin{pmatrix} u_r \\ 0 \\ u_z \end{pmatrix}. \tag{16}$$

From Eq. (12),

$$\frac{1}{2}\rho\frac{\tilde{\mathrm{D}}u_\theta^2}{\mathrm{D}t} = \left(\mathbf{j}_\mathrm{d}\times\mathbf{B}_\mathrm{a}\right)\cdot\mathbf{u}_\theta - \rho\frac{u_r u_\theta^2}{r}, \tag{17}$$

where a swirl velocity, $\mathbf{u}_\theta$, is defined as

$$\mathbf{u}_\theta \equiv \begin{pmatrix} 0 \\ u_\theta \\ 0 \end{pmatrix}. \tag{18}$$

Equation (15) implies that the kinetic energy of the translational motion is gained through the work done by an apparent Lorentz force, $\mathbf{j}_\mathrm{i}\times\mathbf{B}_\mathrm{a}$, in the direction of $\mathbf{u}_{r,z}$. Similarly, based on Eq. (17), the kinetic energy of the swirl motion is gained through the work done by the Lorentz force, $\mathbf{j}_\mathrm{d}\times\mathbf{B}_\mathrm{a}$, in the azimuthal direction. Those kinetic energies are exchangeable through the work done against a centrifugal force, $\rho u_\theta^2 / r$. If the plasma flows in the radially inward direction, that is for $u_r < 0$, the translational energy is transferred to a swirl energy for $u_r > 0$ and vice versa.

Combining Eqs. (15) and (17),

$$\frac{1}{2}\rho\frac{\tilde{\mathrm{D}}u^2}{\mathrm{D}t} = \left(\mathbf{j}_\mathrm{i}\times\mathbf{B}_\mathrm{a}\right)\cdot\mathbf{u}_{r,z} + \left(\mathbf{j}_\mathrm{d}\times\mathbf{B}_\mathrm{a}\right)\cdot\mathbf{u}_\theta. \tag{19}$$

Equation (19) means that the total kinetic energy is the sum of the works done by the resultant Lorentz force. It is reasonably assumed that the plasma flows in a diverging magnetic nozzle with $u_r > 0$, all the input energy is transferred eventually to the kinetic energy in the axial direction. Therefore, the exhaust velocity, U, is given by.

$$\int_{\mathrm{CV}}\frac{1}{2}\rho\frac{\tilde{\mathrm{D}}u^2}{\mathrm{D}t}\mathrm{d}V = \frac{1}{2}\dot{m}U^2. \tag{20}$$

3.2 General formula using effective coefficients

To obtain U and then a thrust, F, the volume integration in Eq. (20) together with Eq. (19) is obtained by introducing the effective coefficients which have an upper bar.

$$\int_{\mathrm{CV}}\left(\mathbf{j}_\mathrm{i}\times\mathbf{B}_\mathrm{a}\right)\cdot\mathbf{u}_{r,z}\mathrm{d}V \equiv \alpha_{\mathrm{ES}}\bar{j}_\mathrm{d}\bar{B}_\mathrm{a}\bar{u}_{r,z}\cdot\pi R_\mathrm{a}^2 L = \alpha_{\mathrm{ES}}\frac{J_\mathrm{d}}{2\pi\frac{R_\mathrm{a}}{2}L}\bar{B}_\mathrm{a}\frac{U}{2}\cdot\pi R_\mathrm{a}^2 L = \frac{\alpha_{\mathrm{ES}}}{2}J_\mathrm{d}\bar{B}_\mathrm{a}UR_\mathrm{a}, \tag{21}$$

$$\int_{\mathrm{CV}} \left(\mathbf{j}_{\mathrm{d}} \times \mathbf{B}_{\mathrm{a}}\right) \cdot \mathbf{u}_{\theta} \mathrm{d}V = \bar{j}_{\mathrm{d}} \bar{B}_{\mathrm{a}} \bar{u}_{\theta} \cdot \pi R_{\mathrm{a}}^2 L = \frac{J_{\mathrm{d}}}{2\pi \frac{R_{\mathrm{a}}}{2} L} \bar{B}_{\mathrm{a}} \bar{u}_{\theta} \cdot \pi R_{\mathrm{a}}^2 L = J_{\mathrm{d}} \bar{B}_{\mathrm{a}} \bar{u}_{\theta} R_{\mathrm{a}}, \tag{22}$$

where we assume that

$$\bar{u}_{\theta} = \alpha_{\mathrm{EM}} \frac{U}{2}. \tag{23}$$

Substituting Eqs. (20) to (23) for Eq. (19),

$$\frac{1}{2} \dot{m} U^2 = \frac{\alpha_{\mathrm{ES}}}{2} J_{\mathrm{d}} \bar{B}_{\mathrm{a}} U R_{\mathrm{a}} + \frac{1}{2} J_{\mathrm{d}} \bar{B}_{\mathrm{a}} \alpha_{\mathrm{EM}} U R_{\mathrm{a}}.$$

Therefore, the thrust, F, is expressed in an electromagnetic form as

$$F = \dot{m} U = \alpha J_{\mathrm{d}} \bar{B}_{\mathrm{a}} R_{\mathrm{a}}, \tag{24}$$

$$\alpha = \alpha_{\mathrm{ES}} + \alpha_{\mathrm{EM}}, \tag{25}$$

$$F_{\mathrm{ES}} \equiv \alpha_{\mathrm{ES}} J_{\mathrm{d}} \bar{B}_{\mathrm{a}} R_{\mathrm{a}}, \tag{26}$$

$$F_{\mathrm{EM}} \equiv \alpha_{\mathrm{EM}} J_{\mathrm{d}} \bar{B}_{\mathrm{a}} R_{\mathrm{a}}, \tag{27}$$

where F_{ES} and F_{EM} are the electrostatic and electromagnetic thrusts, respectively. On the one hand, if a thruster is connected to a constant-voltage power supply as in Hall or stationary plasma thrusters, F is generally determined by a set of three independent operation parameters of $\left(\dot{m}, V_{\mathrm{d}}, \bar{B}_{\mathrm{a}}\right)$; in this case the discharge current, J_{d}, becomes the parameter dependent on them. [34,35]

$$J_{\mathrm{d}} = J_{\mathrm{d}}\left(\dot{m}, V_{\mathrm{d}}, \bar{B}_{\mathrm{a}}\right) \tag{28}$$

On the other hand, if a thruster is connected to a constant-current power supply, another set of operation parameters, $\left(\dot{m}, J_{\mathrm{d}}, \bar{B}_{\mathrm{a}}\right)$, determines F with V_{d} being dependent on them.

Depending on the values of α_{ES} and α_{EM}, the operating modes are categorized as

$$\begin{cases} \text{Electrostatic acceleration mode:} & \alpha_{\mathrm{ES}} \gg \alpha_{\mathrm{EM}} \;\Rightarrow\; \alpha \to \alpha_{\mathrm{ES}},\ F \to F_{\mathrm{ES}} \\ \text{Electromagnetic acceleration mode:} & \alpha_{\mathrm{ES}} \ll \alpha_{\mathrm{EM}} \;\Rightarrow\; \alpha \to \alpha_{\mathrm{EM}},\ F \to F_{\mathrm{EM}} \\ \text{Hybrid acceleration mode:} & \alpha_{\mathrm{ES}} \simeq \alpha_{\mathrm{EM}} \end{cases}.$$

Next, let F be expressed using $\left(\dot{m}, V_{\mathrm{d}}\right)$. Here, we assume that the azimuthal current is induced only by the $\mathbf{E}\times\mathbf{B}$ drift of the electrons.

$$\bar{j}_\theta = \bar{n}e\frac{\bar{E}}{\bar{B}_\mathrm{a}} = \alpha_\mathrm{ES}\bar{j}_\mathrm{d} = \alpha_\mathrm{ES}\frac{J_\mathrm{d}}{2\pi\frac{R_\mathrm{a}}{2}L} = \alpha_\mathrm{ES}\frac{J_\mathrm{d}}{\pi R_\mathrm{a}L}. \tag{29}$$

From Eqs. (24), (25), and (29),

$$F = \dot{m}U = \left(\alpha_\mathrm{ES}+\alpha_\mathrm{EM}\right)\bar{n}e\frac{\bar{E}}{\bar{B}_\mathrm{a}}\frac{\pi R_\mathrm{a}L}{\alpha_\mathrm{ES}}\bar{B}_\mathrm{a}R_\mathrm{a} = \left(1+\frac{\alpha_\mathrm{EM}}{\alpha_\mathrm{ES}}\right)\bar{n}e\bar{E}\pi R_\mathrm{a}^2L. \tag{30}$$

Since

$$\dot{m} = m\bar{n}\,\bar{u}_z\pi R_\mathrm{a}^2, \tag{31}$$

$$\bar{E} = \beta_1\frac{V_\mathrm{d}}{R_\mathrm{a}},\ \beta_1 \simeq 1, \tag{32}$$

$$F = \left(1+\frac{\alpha_\mathrm{EM}}{\alpha_\mathrm{ES}}\right)\frac{\dot{m}}{m\bar{u}_z\pi R_\mathrm{a}^2}e\beta_1\frac{V_\mathrm{d}}{R_\mathrm{a}}\pi R_\mathrm{a}^2L = \left(1+\frac{\alpha_\mathrm{EM}}{\alpha_\mathrm{ES}}\right)\beta_1\frac{e\dot{m}}{m}\frac{1}{\bar{u}_z}\frac{L}{R_\mathrm{a}}V_\mathrm{d}. \tag{33}$$

Assume

$$\bar{u}_z = \beta_2 U,\ 0<\beta_2<1, \tag{34}$$

$$F = \dot{m}U = \alpha'\dot{m}\sqrt{\frac{e}{m}V_\mathrm{d}}, \tag{35}$$

$$\alpha' \equiv \sqrt{\left(1+\frac{\alpha_\mathrm{EM}}{\alpha_\mathrm{ES}}\right)\frac{\beta_1}{\beta_2}\frac{L}{R_\mathrm{a}}}. \tag{36}$$

For a given value of m that depends on the propellant species, Eq. (35) gives the thrust using $\left(\dot{m},V_\mathrm{d}\right)$. It is noteworthy that α' depends on $\bar{B}_\mathrm{a}$. Therefore, F is a function of $\left(\dot{m},V_\mathrm{d},\bar{B}_\mathrm{a}\right)$ in its general form.

Equations (24) and (35) are compatible with each other, giving the thrust as a function of $\left(\dot{m},V_\mathrm{d},\bar{B}_\mathrm{a}\right)$ in different forms. Equation (24) is in a traditional, electromagnetic acceleration form that has been used for MPD thrusters; the thrust is expressed using J_d and $\bar{B}_\mathrm{a}$, not explicitly using $\dot{m}$. Equation (35) is an electrostatic acceleration form that has typically been used in ion and Hall thrusters; the thrust is expressed using $\dot{m}$ and V_d, not explicitly using $\bar{B}_\mathrm{a}$.

4. Experimental results and discussions

In this study, we analyse experimental data obtained using three thrusters. All the thrusters have axisymmetric configurations composed of a hollow cathode on the centre axis, and an anode made of copper surrounding it. The electrodes are separated by an insulator. An external magnetic field is applied using either an electromagnet or a permanent magnet. The strength of the applied magnetic field is represented by the value at the centre of the solenoid coil/permanent magnet on the centre axis, $\bar{B}_a$. One of them is categorized as an applied-field magnetoplasmadynamics thruster (AF‐MPD), which is recognized as the electromagnetic acceleration type; the other two are our original type, central-cathode, electrostatic thrusters (CC-EST-1 and CC-EST-2) in which we claim that electrostatic-magnetic hybrid acceleration is realized. The thrust performance data were obtained using a 2-m-diameter, 4-m-long stainless-steel vacuum chamber with a turbo-molecular pump (3200 L/s) backed by a rotary pump (33.3 L/s) for the AF‐MPD and CC‐EST‐1, or using a 1.2-m-diameter, 3.2-m-long, stainless-steel vacuum chamber with a cryogenic pump (8400 L/s for argon, 4600 L/s for xenon) backed by a dry pump (116.7 L/s) for the CC-EST-2. The thruster is mounted on a pendulum-type thrust stand. The details of the method of thrust measurement are described in Refs. [33,48,57]

The thruster operation conditions are shown in Table 1. In the case of AF-MPD, argon is used as the propellant. In the case of CC‐ESTs, operation with argon was examined, resulting in unstable operation and poor thrust performance. Therefore, the thrust characteristics of only xenon are evaluated in this study. The same species as of the propellant was used as the working gas of the hollow cathode.

Table 1 Thruster operating conditions

Type	$\bar{R}_a$ [mm]	Propellant		Cathode working gas		$\bar{B}_a$ [mT]	V_d [V]	J_d [A]
		Species	$\dot{m}_a$ [mg/s] ([Aeq.])	Species	$\dot{m}_c$ [mg/s] ([Aeq.])			
AF–MPD	40	Ar	0 (0)	Ar	0.83–2.08 (2.00–5.00)	133–265	–	10–60
CC–	40	Xe	0.68–2.05	Xe	0.49	100–250	80–250	–

EST–1			(0.5–1.5)		(0.36)			
CC–EST–2	15	Xe	0.68–4.77 (0.5–3.5)	Xe	0.49 (0.36)	210–402	100–300	–

4.1. Applied-field MPD thruster

Figure 3 schematically illustrates the applied‑field MPD thruster examined in this study. It has an annular anode made of copper, composed of a conical section and an 80 mm inner diameter cylindrical one, and a hollow cathode on the centre axis. These electrodes are assembled with a cylindrical insulator made of alumina. The hollow cathode was either a commercial product (Kaufmann & Robinson Inc., LHC–03–AE1–01, 20 A maximum) [58] included in the figure [48] or a self-developed one made of lanthanum hexaboride (LaB6, optional). [59] The electrodes are connected to a constant-current power supply. Using a solenoid coil (inner diameter = 100 mm; outer diameter = 210 mm, length = 100 mm), a slowly‑diverging magnetic nozzle is formed.

All of the data included in the figure were obtained by analysing the existing data. [48,59] In the experiment of this study, argon was used as the propellant, being injected only from the hollow cathode tip. Experimentally measured thruster characteristics AF-MPD are shown in Figs. 4a and 4b. As seen in Fig. 4a, the thrust characteristics of the AF-MPD do not fit well to the electrostatic acceleration form of Eq.(35) Since the thrust is generated mostly by the electromagnetic acceleration, in which F is independent of $\dot{m}$. Since the propellant is injected only from the cathode tip, the propellant flow does not experience the potential drop applied between the anode and cathode. As seen in Fig. 4b, the thrust fits well to the electromagnetic acceleration form of Eq. (24) with the value of the coefficient, α, being about 0.16.

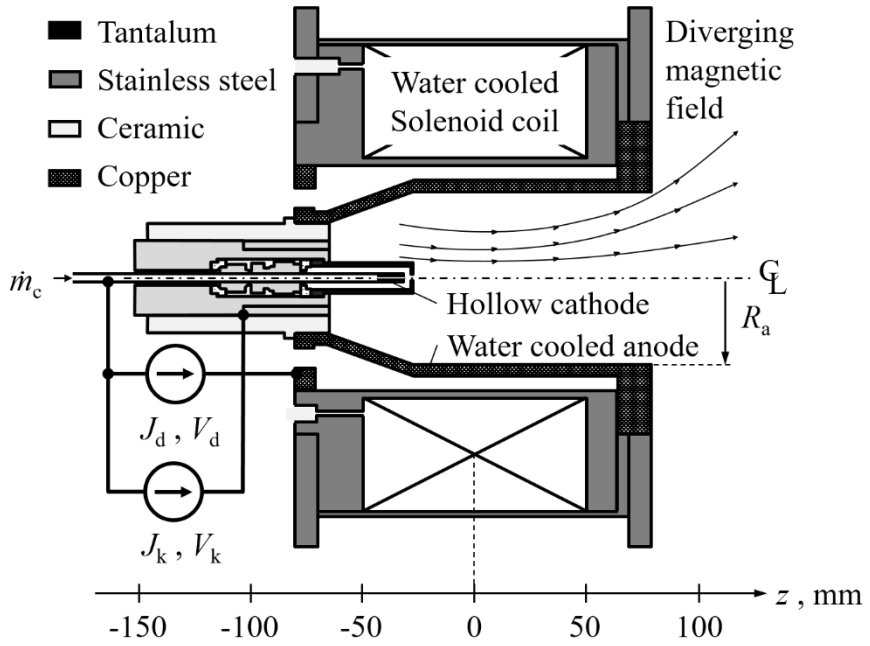

Fig. 3 Schematic illustration of AF-MPD with nominal hollow cathode, Ref. [48]

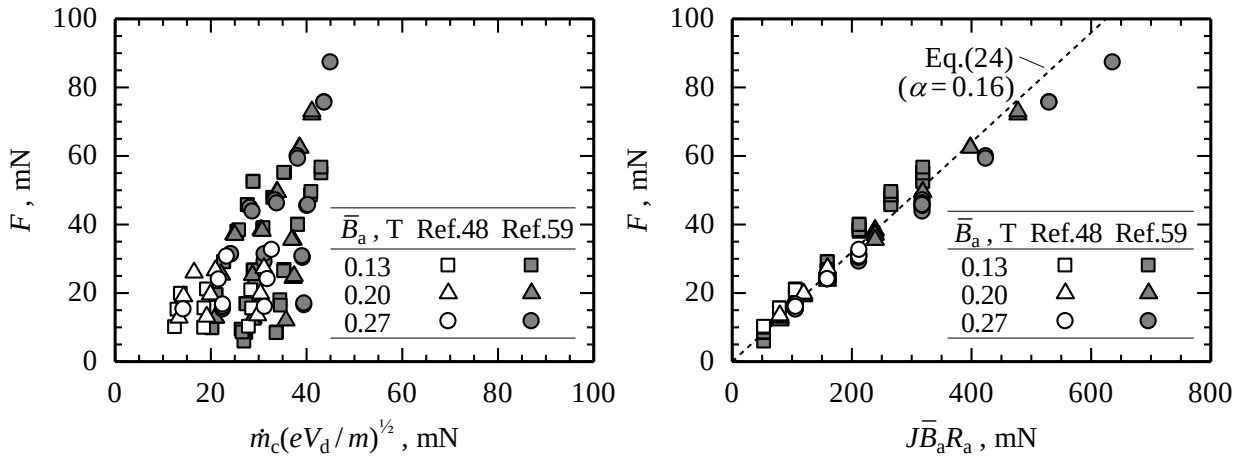

a) F vs. $\dot{m}_c\left(eV_d/m\right)^{1/2}$ b) F vs. $J\bar{B}_aR_a$

Fig. 4 Thrust characteristics of AF-MPD.

4.2. Central-cathode electrostatic thrusters (CC-EST)

Next, we will present thrust characteristics of our original thruster, CC-EST. [33] As will be demonstrated, we examined two configurations. Both of them have the common, basic configuration as of Fig. 2. Unlike AF-MPD, the propellant is supplied along the inner surface of a ring anode, thereby expecting that the injected propellant is ionized near the anode, and the ions so produced are accelerated by the potential drop between the anode and that on the centre axis where the potential is expected nearly at the cathode level.

4.2.1. CC–EST–1

Figure 5 schematically illustrates the cross-sectional view of CC-EST-1. [33] In this model, only a short portion of the inner surface of a copper ring with an inner radius of R_a (= 40 mm) and a length L_a (= 8 mm) is exposed to the discharge zone as an effective anode. The propellant, xenon, is injected along the anode's inner surface from a 1.5-mm-thick annular slit. A slowly diverging magnetic field is applied using a solenoid coil. A hollow cathode (Kaufmann & Robinson Inc., LHC–03–AE1–01, 20 A maximum) is set on the centre axis with the axial location of its tip at the centre of the solenoid coil. The electrodes are assembled with an insulator made of alumina. The electrodes are connected to a constant voltage power supply. $\bar{B}_a$ is a variable with varying current on the solenoid coil (inner diameter = 100 mm; outer diameter = 210 mm, length = 100 mm). As shown in Fig. 5, the magnetic field is shaped as a slowing diverging magnetic nozzle without a cusp. Previous series of thrust characteristics data measured using this thruster are already published in Ref. [33]. New sets of data are presented in this study.

As seen in Fig. 6a, the thrust characteristics of CC-EST-1 fit well to the electrostatic thrust form of Eq. (35) irrespective of the value of $\bar{B}_a$ with the value of the coefficient, α', of 0.99 with a coefficient of determination of 0.89. The characteristics are consistent with the ion acceleration scenario in CC-EST that the propellant is ionized near the anode and then experiences the electrostatic acceleration between the potential drop from the anode to that on the centre axis. Figure 6b shows thrust characteristics in the electromagnetic form. F roughly fits to Eq. (24). However, the value of α depends on $\bar{B}_a$, ranging between 0.55 to 0.76. This issue will be further discussed later.

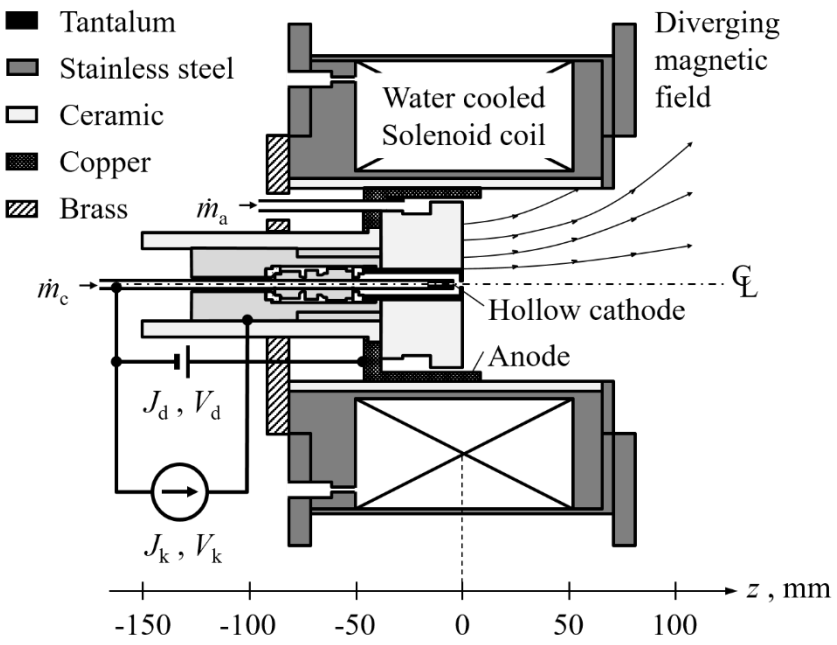

Fig. 5 Schematic illustration of CC-EST-1

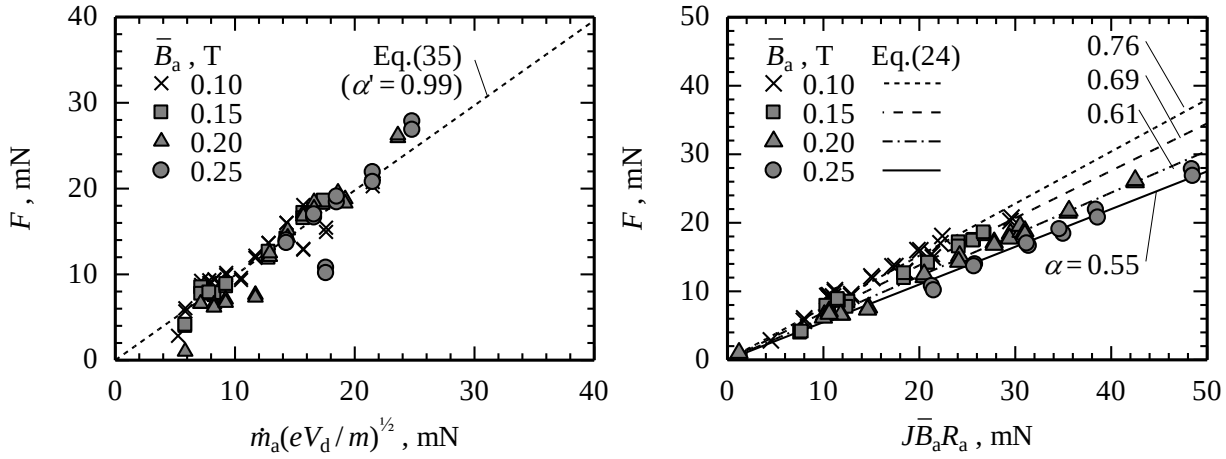

a) F vs. $\dot{m}_a\left(eV_d/m\right)^{1/2}$

b) F vs. $J\bar{B}_aR_a$, best fit values of α are 0.76, 0.69, 0.61 and 0.55 for $\bar{B}_a$ = 0.10 T, 0.15 T, 0.21 T and 0.25 T, respectively.

Fig. 6 Thrust characteristics of CC-EST-1.

4.2.2. CC-EST-2

CC-EST-2, Fig. 7, is the thruster newly developed in this study. As in CC-EST-1, it also has a ring anode made of copper and a hollow cathode (Kaufmann & Robinson Inc., LHC–03–AE1–01) on the centre axis. An external magnetic field is applied using a permanent ring magnet with an outer diameter of 100 mm and a thickness of 30 mm. It is packed in a housing made of stainless steel (ISO 4401-316-00-I or JIS SUS316), which in turn is covered against the plasma with an insulator wall made of photoveel. $\bar{B}_a$ was varied to three values using different permanent magnet materials and inner diameters; $\bar{B}_a$ = 210 mT with Ferrite and inner diameter of 58 mm, $\bar{B}_a$ = 315 mT with SmCo and inner diameter of 45 mm, and $\bar{B}_a$ = 402 mT with Neodymium (NdFeB) and inner diameter of 45 mm. In order to reduce the total mass including the permanent magnet, the inner diameter of the anode ring is reduced to R_a = 15 mm, while its exposed length L_a is unchanged (= 8 mm). The propellant is fed through the 1.5-mm-thick slit between the anode inner surface and the insulator. Unlike the case of using a solenoid coil, the applied magnetic field has a cusp around the exit of the thruster over the insulator wall. However, the ion acceleration is expected to be almost completed in the region upstream from the cusp.

As shown in Fig. 8a, irrespective of the value of $\bar{B}_a$, F is also well fit to the electrostatic thrust of Eq. (35). The value of α' (=0.97) is close to that of CC-EST-1, the coefficient of determination of 0.97. In the thrust characteristics in the electromagnetic form shown in Fig. 8b, F roughly fit to the linear relation of Eq. (24). However, the fit values of α also depend on $\bar{B}_a$, at a higher level, from 0.92 to 1.18, than that of CC-EST-1.

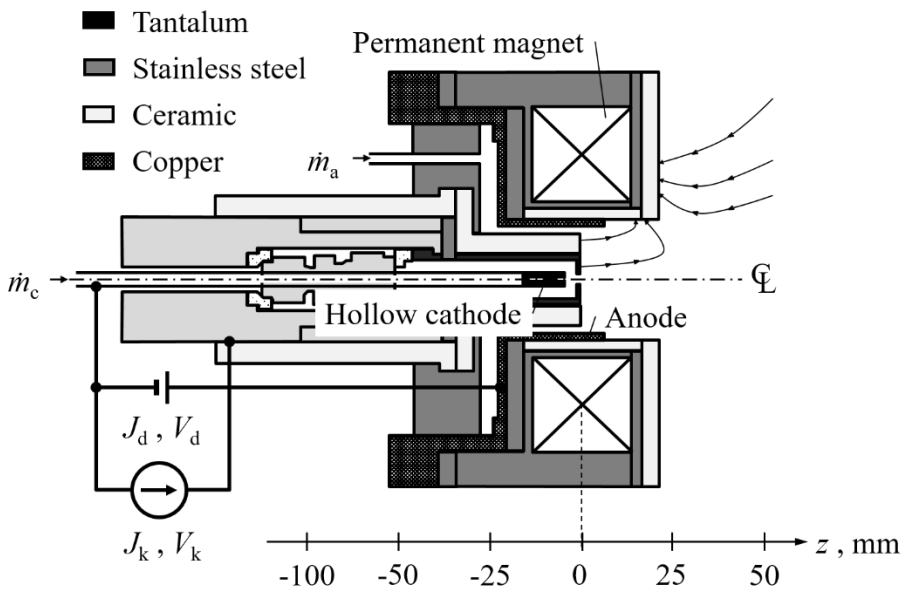

Fig. 7 Schematic illustration of CC-EST-2

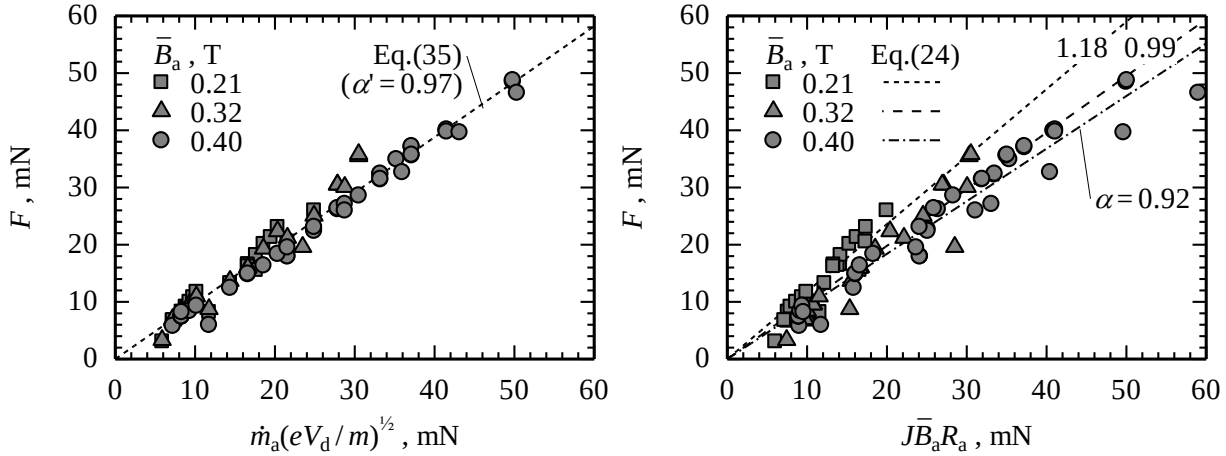

a) F vs. $\dot{m}_a\left(eV_d/m\right)^{1/2}$

b) F vs. $J\bar{B}_aR_a$, best fit values of α are 1.18, 0.99 and 0.92 for $\bar{B}_a$ = 0.21 T, 0.32 T and 0.40 T, respectively.

Fig. 8 Thrust characteristics of CC-EST-2.

4.2.3 Evaluation of electrostatic and electromagnetic thrust components

The contributions of the electrostatic and electromagnetic thrusts can be compared by evaluating α_{ES} and α_{EM}. To quantify the respective contributions in the experimentally measured thrust characteristics, we analysed the dependence of α_{ES} on $\bar{B}_{\mathrm{a}}$. From Eq. (29),

$$\alpha_{\mathrm{ES}} = \bar{n}e\frac{\bar{E}}{\bar{B}_{\mathrm{a}}}\frac{\pi R_{\mathrm{a}} L}{J_{\mathrm{d}}} = \frac{\bar{n}e\bar{E}\pi R_{\mathrm{a}}^2 L}{J_{\mathrm{d}}\bar{B}_{\mathrm{a}} R_{\mathrm{a}}}. \tag{37}$$

The numerator of the rightmost side of Eq. (37), that is F_{ES} given by Eq. (26), equals the volume integration of the electrostatic force, which in principle should be independent of $\bar{B}_{\mathrm{a}}$. Here, we simplify Eq. (37) as

$$\alpha_{\mathrm{ES}} = \frac{\bar{B}_{\mathrm{a,c}}}{\bar{B}_{\mathrm{a}}},\ \bar{B}_{\mathrm{a,c}}=\text{const.} \tag{38}$$

Substituting Eq. (38) for Eq. (25),

$$\alpha = \frac{\bar{B}_{\mathrm{a,c}}}{\bar{B}_{\mathrm{a}}} + \alpha_{\mathrm{EM}}. \tag{39}$$

It follows from the results above that Eq. (24) is expressed as the sum of the electrostatic and electromagnetic components:

$$F = F_{\mathrm{ES}}\left(\dot{m}, V_{\mathrm{d}}\right) + F_{\mathrm{EM}}\left(J_{\mathrm{d}}, \bar{B}_{\mathrm{a}}\right). \tag{40}$$

The electrostatic thrust, F_{ES}, depends on a set of only two parameters of $\left(\dot{m}, V_{\mathrm{d}}\right)$, not being dependent on $\bar{B}_{\mathrm{a}}$. The electromagnetic thrust, F_{EM}, depends on a set of only two parameters of $\left(J_{\mathrm{d}}, \bar{B}_{\mathrm{a}}\right)$. However, that in a constant–voltage operation, F_{EM} still depends on $\dot{m}$ and V_{d} because J_{d} is dependent on them.

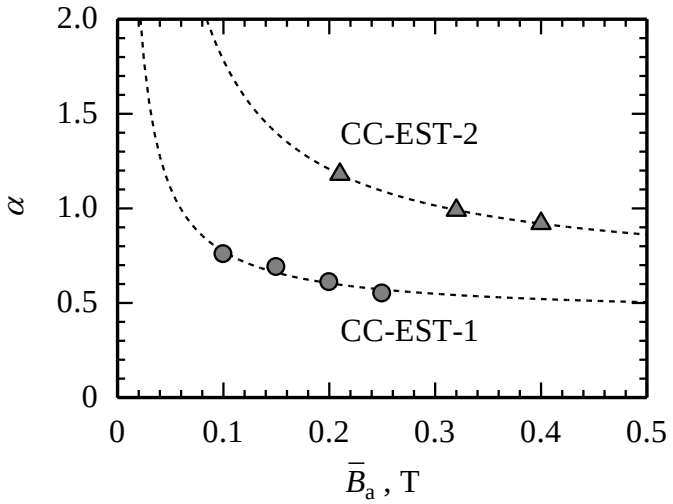

Fig. 9 α vs. $\bar{B}_a$

Table 2 Experimentally fitted values

Type	$\bar{B}_{a,c}$ [T]	α_{ES}	α_{EM}	α
AF–MPD	0.00	0.00	0.16	0.16
CC–EST–1	0.04	0.16–0.40	0.39	0.55–0.80
CC–EST–2	0.11	0.28–0.52	0.64	0.92–1.18

In the EST operations shown above, we can set a thruster's operating conditions using three independent operation parameters, $\dot{m}$, V_d, and $\bar{B}_a$; J_d is dependent on them, that is $F = F\left(\dot{m}, V_d, \bar{B}_a\right)$. However, the dependencies of F_{ES} and F_{EM} on $\bar{B}_a$ are different. As shown in Eq. (39), while α_{EM} does not depend on $\bar{B}_a$, α_{ES} is in inversely proportional to it. The values of $\bar{B}_{a,c}$ and α_{EM} were obtained by fitting the experimental performance of each thruster type to Eq. (39), see Fig. 9. The results are presented in Table 2. In both CC-EST-1 and -2, the electrostatic and electromagnetic thrusts are of the same order. However, in AF-MPD, the electrostatic thrust is negligible. From these results, we conclude that in CC-EST-1 and -2, the electrostatic-magnetic-hybrid acceleration is realized, whereas with AF–MPD only the electromagnetic thrust is dominant.

5. Conclusion

An electrostatic-magnetic-hybrid acceleration has been achieved using a central-cathode electrostatic thruster (CC-EST), in which the propellant injected along the anode's inner surface is expected to be ionized near the inlet and accelerated through the applied potential drop. The thruster's operating condition is determined using three independent parameters, $\dot{m}_a$, V_d, and $\bar{B}_a$. The thrust, comprising electrostatic and electromagnetic components, is formulated based on continuum single-fluid conservation equations applied over the acceleration zone. The electrostatic component depends on $\dot{m}_a$ and V_d, but is independent of $\bar{B}_a$. Conversely, the electromagnetic component is a function of a discharge current, J_d, and $\bar{B}_a$, where J_d is determined by all three operation parameters. The experimentally measured thrust characteristics are reasonably fit to the thrust formula. The contributions of the respective thrust components are evaluated by utilizing the above-mentioned difference in $\bar{B}_a$ dependence, and in the CC-EST operations that are evaluated to be comparable. This electrostatic-magnetic-hybrid thrust generation in the CC-ESTs is a promising way to widen the variety in electric propulsion options suitable for high-thrust-density with a simple magnetic circuit.

Acknowledgments

The authors thank Mr. A. Saito, Technical Division, Nagoya University for his valuable technical assistance. This research was supported by the Japan Society for Promotion of Science, Grant–in–Aid for Scientific Research (A), No. 15H02321, and by Mitsubishi Heavy Industries, Ltd., Tokyo, Japan.

References

[1] http://boeing.mediaroom.com/2015–09–10–Boeing–World–s–First–All–Electric–Propulsion–Satellite–Begins–Operations#assets_117 (as of July 8, 2018)

[2] http://news.eutelsat.com/pressreleases/eutelsats–airbus–built–full–electric–eutelsat–172b–satellite–reaches–geostationary–orbit–2208095 (as of July 8,2018)

[3] K. Lemmer, Propulsion for CubeSats, Acta Astronaut. 134 (2017) 231–243.

[4] I. Levchenko et al., Space Micropropulsion Systems for Cubesats and Small Satellites: From Proximate Targets to Furthermost Frontiers, Appl. Phys. Rev. 5 (2018) 011104.

[5] I. Levchenko et al., Recent Progress and Perspectives of Space Electric Propulsion Systems based on Smart Nanomaterials, Nat. Commun. 9 (2018) 879.

[6] R. Jahn, Physics of Electric Propulsion, McGraw‑Hill, New York, 1968, Chaps. 6‑8.

[7] D. M. Goebel, I. Katz, Fundamentals of Electric Propulsion: Ion and Hall Thrusters, JPL Space Science and Technology Series, Jet Propulsion Laboratory, California Institute of Technology, 2008, Chaps. 1, 2.

[8] F. F. Chen, Introduction to Plasma Physics and Controlled Fusion, second ed., Plenum Press, New York, Sec. 8.2.4, 1984.

[9] J. M. Sankovic, J. A. Hamley, T. W. Haag, Performance Evaluation of the Russian SPT Thruster at NASA LeRC, 23th International Electric propulsion Conference, Seattle, IEPC‑1993–094, 1993.

[10] D. Manzella, C. Sarmiento, J. Sankovic, T. Haag, Performance Evaluation of the SPT–140, 25th International Electric propulsion Conference, Cleveland, Ohio, IEPC‑1997–059, 1997.

[11] A. I. Morozov and V. V. Savelyev, *Fundamentals of Stationary Plasma Thruster Theory* (Springer, New York, 2000) p. 203–391.

[12] I. G. Mikellides, I. Katz, R. R. Hofer and D. M. Goebel, Magnetic Shielding of a Laboratory Hall Thruster. I. Theory and validation, J. Appl. Phys. 115, 043303 (2014).

[13] Y. Raitses and N. J. Fisch, Parametric Investigations of a Nonconventional Hall Thruster, Phys. Plasmas 8 (2001) 2579–2586.

[14] K. D. Diamant, J. E. Pollard, Y. Raitses, and N. J. Fisch, Ionization, Plume Properties, and Performance of Cylindrical Hall Thrusters, IEEE Trans. Plasma Sci. 38 (2010) 1052–1057.

[15] N. Koch, H. P. Harmann and G. Kornfeld, Development & Test Status of the THALES High Efficiency Multistage Plasma (HEMP) Thruster Family, in Proceedings of the 29th International Electric Propulsion Conference, IEPC Paper No. 2005–297, Princeton, USA, 2005.

[16] N. Koch, H.‐P. Harmann, G. Kornfeld, Status of the THALES High Efficiency Multi Stage Plasma Thruster Development for HEMP–T 3050 and HEMP–T 30250, 30th International Electric Propulsion Conference, Florence, Italy, IEPC‐2007‐100, 2007.

[17] S. Harada, T. Baba, A. Uchigashima, S. Yokota, A. Iwakawa, A. Sasoh, T. Yamazaki & H. Shimizu, Electrostatic Acceleration of Helicon Plasma using a Cusped Magnetic Field. Appl. Phys. Lett. 105, 194101 (2014).

[18] D. Ichihara, A. Uchigashima, A. Iwakawa, A. Sasoh, Electrostatic Ion Acceleration Across a Diverging Magnetic Field, Appl. Phys. Lett. 109 (2016) 053901.

[19] D. Ichihara, A. Iwakawa, A. Sasoh, Effects of Magnetic Field Profile Near Anode On Ion Acceleration Characteristics of a Diverging Magnetic Field Electrostatic Thruster, J. Appl. Phys. 122 (2017) 043302.

[20] G. Krulle, M. Auweter–Kurtz, A. Sasoh, Technology and Application Aspects of Applied Field Magnetoplasmadynamic Propulsion, J. Propul. Power 14 (1998) 754–763.

[21] K. Dannenmayer, S. Mazouffre, Elementary Scaling Relations for Hall Effect Thrusters, J. Propul. Power 27 (2011) 236–245.
doi: 10.2514/1.48382

[22] K. Sankaran, L. Cassady, A. D. Kodys, E. Y. Choueiri, A Survey of Propulsion Options for Cargo and Piloted Missions to Mars, Annals of the New York Academy of Sciences 1017 (2006) 450–467.

[23] E. Y. Choueiri, A Critical History of Electric Propulsion: The First 50 Years (1906–1956), J. Propul. Power 20 (2004) 193–203.

[24] H. Maecker, Plasmaströmungen in Lichtbögen infolge eigenmagnetischer Kompression, Z. Phys. 141 (1) (1955).

[25] E. Choueiri, Scaling of Thrust in Self–Field Magnetoplasmadynamic Thrusters, J. Propul. Power 14 (1998) 744–753.

[26] D. B. Fradkin, A. W. Blackstock, D. J. Roehling, T. F. Stratton, M. Williams, K. W. Liewer, Experiments Using a 25–kW Hollow Cathode Lithium Vapor MPD Arcjet, AIAA J. 8 (1970) 886–894.

[27] H. Hügel, Self‐Magnetic Effect in Arcjet Engine, AIAA J. 6(8) (1968) 1573‐1575.

[28] V. B. Tikhonov, S. Semenikhin, J. R. Brophy, J. E. Polk, The Experimental Performance of the 100 kW Li MPD Thruster with External Magnetic Field, 24th International Electric Propulsion Conference, IEPC–95–105, 1995.

[29] V. B. Tikhonov, S. A. Semenikhin, J. E. Polk, Own Magnetic Field Impact on MPD Thrusters Performance with External Magnetic Field, 26th International Electric Propulsion Conference, IEPC‑99‑176, 1999.

[30] A. Sasoh, Y. Arakawa, Thrust Formula for Applied-Field Magnetoplasmadynamic Thrusters Derived from Energy Conservation Equation, J. Propul. Power, 11 (1995) 351–356.

[31] A. Sasoh, Simple Formulation of Magnetoplasmadynamic Acceleration, Phys. Plasmas 1 (1994) 464–469.

[32] M. Coletti, A Thrust Formula for an MPD Thruster with Applied–magnetic Field, Acta Astronaut. 81 (2012) 667–674.

[33] A. Sasoh, K. Mizutani, A. Iwakawa, Electrostatic/magnetic Ion Acceleration Through a Slowly Diverging Magnetic Nozzle between a Ring Anode and an On–axis Hollow Cathode, AIP Advances 7 (2017) 065204.

[34] H. Kim, W. Choe, Y. Lim, S. Lee, S. Park, Magnetic Field Configurations on Thruster Performance in Accordance with Ion Beam Characteristics in Cylindrical Hall Thruster Plasmas, Appl. Phys. Lett. 110 (2017) 114101.

[35] Y. Gao, H. Liu, P. Hu, H. Huang, D. Yu, The Effect of Magnetic Field near the Anode on Cylindrical Hall Thruster, Plasma Sources Sci. Tech. 25 (2016) 035011.

[36] Y. Gao, H. Liu, P. Hu, H. Huang, D. Yu, Effect of Anode Position on the Performance Characteristics of a Low–power Cylindrical Hall Thruster, Phys. Plasmas 24 (2017) 063518.

[37] N. M. Nerheim, A. J. Kelly, A Critical Review of the Magnetoplasmadynamic (MPD) Thruster for Space Applications, NASA TR–32–1196, 1968.

[38] R. J. Sovie, D. J. Connolly, Effect of Background Pressure on Magnetoplasmadynamic Thruster Operation, J. Spacecraft Rockets 7 (1970) 255–258.

[39] I. Kimura, Y. Arakawa, Effect of Applied Magnetic Fields on Physical Processes in an MPD Arcjet, AIAA J. 15(1977) 721–724.

[40] Y. Arakawa, A. Sasoh, Steady–State Permanent Magnet Magnetoplasmadynamic Thruster, J. Propul. Power 5 (1989) 301–304.

[41] A. Sasoh, Y. Arakawa, Electromagnetic Effects in an Applied–Field Magnetoplasmadynamic Thruster, J. Propul. Power 8 (1992) 98–102.

[42] R. M. Myers, Geometric Scaling of Applied–Field Magnetoplasmadynamic Thrusters, J. Propul. Power 11 (1995) 343–351.

[43] H. Tahara, Y. Kagaya, T. Yoshikawai, Effects of Applied Magnetic Fields on Performance of a Quasisteady Magnetoplasmadynamic Arc, J. Propul. Power 11 (1995) 337–342.

[44] H. Tahara, Y. Kagaya, T. Yoshikawa, Performance and Acceleration Process of Quasisteady Magnetoplasmadynamic Arcjets with Applied Magnetic Fields, J. Propul. Power 13 (1997) 651–658.

[45] P. G. Mikellides, P. J. Turchi, N. F. Roderick, Applied–Field Magnetoplasmadynamic Thrusters, Part 1: Numerical Simulations Using the MACH2 Code, J. Propul. Power 16 (2000) 887–893.

[46] D. R. Lev, Investigation of Efficiency in Applied Field Magnetoplasmadynamic Thrusters, Ph. Dissertation, The Department of Mechanical and Aerospace Engineering, Princeton University, Princeton, 2012.

[47] R. Albertoni, F. Paganucci, P. Rossetti, M. Andrenucci, Experimental Study of a Hundred–Kilowatt–Class Applied–Field Magnetoplasmadynamic Thruster, J. Propul. Power 29（2013) 1138–1145.

[48] D. Ichihara, T. Uno, H. Kataoka, J.‑H. Jeong, A. Iwakawa, A. Sasoh, Ten–Ampere–Level, Applied–Field–Dominant Operation in Magnetoplasmadynamic Thrusters, J. Propul. Power 33 (2017) 360–369.

[49] R. Albertoni, F. Paganucci, M. Andrenucci, A Phenomenological Performance Model for Applied–Field MPD Thrusters, Acta Astronaut. 107 (2015) 177–186.

[50] A. Boxberger, G. Herdrich, Integral Measurements of 100 kW Class Steady State Applied–Field Magnetoplasmadynamic Thruster SX3 and Perspectives of AF–MPD Technology, 35th International Electric Propulsion Conference, Atlanta, IEPC–2017–339, 2017.

[51] B. Wang, H. Tang, Z. Li, X. Lu, Z. Zhang, Research on Current Outflow in the Plasma Beam of a Low Power Applied–field Magnetoplasmadynamic Thruster, 35th International Electric Propulsion Conference, Atlanta, IEPC–2017–299, 2017.

[52] H. R. Kaufman, R. S. Robinson, R. I. Seddon, End–Hall ion source, J. Vacuum Sci. Tech. A 5 (1987) 2081–2084.

[53] Y. Ding, H. Sun, L. Wei, P. Li, H. Su, W. Peng, D. Yu, A 200 W Hall Thruster with Hollow Indented Anode, Acta Astronaut. 139 (2017) 521–527.

[54] J. Duras1, D. Kahnfeld, G. Bandelow, S. Kemnitz, K. Lüskow, P. Matthias, N. Koch, R. Schneider, Ion angular distribution simulation of the Highly Efficient Multistage Plasma Thruster, J. Plasma Phys. 83 (2017) 595830107.

[55] G. W. Sutton, A. Sherman, Engineering Magnetoplasmadynamics, McGraw‑Hill, New York, Sec. 8.2, 1965.

[56] K. K. Kuo, Principles of Combustion, John Wiley & Sons, Hoboken, New Jersey, U. S. A., p.312, 2005.

[57] A. Sasoh, Y. Arakawa, A High–Resolution Thrust Stand for Ground Tests of Low–Thrust Space Propulsion Devices, Rev. Sci. Instrum. 64 (1993) 719–723.

[58] H. R. Kaufman, J. R. Kahn, Hollow Cathode without Low–Work–Function Insert, 29th International Electric Propulsion Conference, IEPC‑2005–47, 2005.

[59] H. Kasuga, J.‑H. Jeong, K. Mizutani, A. Iwakawa, A. Sasoh, K. Kojima, T. Kimura, Y. Kawamata, M. Yasui, Operation Characteristics of Applied‑Field Magnetoplasmadynamics Thruster Using Hollow Cathode, Aerospace Tech. Japan T. Jpn Soc. Aeronaut. S. 16 (2018) 69–74.